Millimeter-wave Wireless Communication in a Data Center Cabinet with Adaptive Control of Propagation

Julian Webber, Hirokazu Kamoda, Naoya Kukutsu and Tomoaki Kumagai
Advanced Telecommunications Research Institute International, 2-2-2, Hikaridai, Seika-cho, Kyoto, 619-0288, Japan
{**jwebber, t.kumagai**}**@atr.jp**

***Abstract*—A 60 GHz wireless communication system has been proposed as a replacement for data cables in a data-center cabinet in order to reduce the significant cooling energy costs. This paper investigates the feasibility of placing adaptive absorber-reflector regions on the sides of a cabinet as a static channel fading counter-measure and also to optimize performance for a particular server. As a result of a ray-tracing simulation it is shown that the capacity could be increased by 2.8 bits/s/Hz at an SNR of 20 dB at the median value.**

***Keywords*—**data-center, 60 GHz, adaptive/active control of propagation, ray-tracing, capacity, meta-material

I. Introduction

The world-wide total energy consumption of data-centers was about 270 TWh in 2012 which represented about 2% of the global power consumption [1]. This figure was further predicted to grow annually by about 4.3%. A significant portion of this energy is attributable to the air-conditioning equipment, and in efforts to reduce this value, 'green' data-centers are an expanding research area.

In the front section of a typical data-center cabinet there is a total of several tens of meters of Cat. 6 Ethernet cable connecting typically 40 servers to a central L2/L3 switch [2]. This cabling substantially impedes proper air-flow and hence increases the cooling energy costs. The 60 GHz band which offers a wide bandwidth, has been identified as an alternative communications technology that will soon be widely used and cost-effective. Cable replacement also simplifies data-center maintenance including rerouting of server connections whenever necessary.

Since the arrival of green low-power Ethernet devices, the power consumption per port has decreased rapidly. In the current state-of-the-art switches for data-centers, the typical power consumption per 10 Gigabit Ethernet port is less than 3.5 W and each 40 Gigabit Ethernet port consumes less than 14 W [3]. However, it is the additional cooling costs that are a significant part. Meanwhile, recent CMOS 60 GHz transceivers have been reported having Tx mode power consumptions of 170 mW (90 mm) [4], and 252 mW (65 mm) [5].

Recently, a number of research papers have described data-center inter-cabinet communications using line-of-sight (LOS) links at 60 GHz, for example [6] [7] [8]. However, there has been comparatively little work published on intra-cabinet communications between the L2/L3 switch and each server, which at mm-wave brings new challenges. A high-data rate

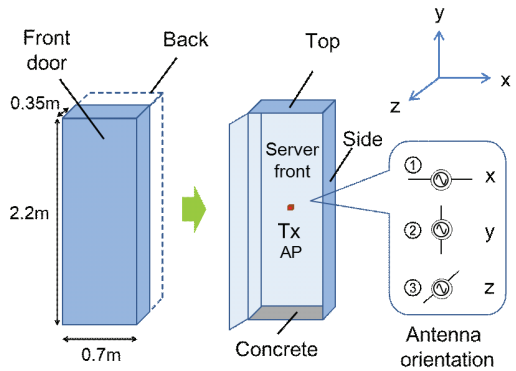

Fig. 1. Dimensions of front space of data center cabinet and access point (Tx) and Rx antenna orientation.

orthogonal frequency division multiplexing (OFDM) 60 GHz communications system for use in a metallic enclosed typographical machine was described in [9]. In this paper we propose a technique to increase the capacity of the intra-cabinet data-center communication using adaptive control of reflector material.

60 GHz communication is characterized by high path-loss caused by oxygen-absorption and communications are generally short range using low-transmit powers. The cabinet's metallic construction promotes the generation of multiple delayed reflections thus creating a frequency selective channel. In normal operation when the front access door is closed, the wireless channel is essentially static, although there will be small channel variations over time caused by temperature variation and material expansion. A range of capacities will be realized depending on the exact location of each servers' antenna. However, precise positioning of elements to avoid fading is not practical during the cabinet design because of the short mm-wavelengths. Although the received signal strength can be increased by employing antenna diversity using an RF switch connected to additional antenna elements, there are significant power losses at 60 GHz associated with this method. Employing extra RF chains is also a costly solution both in terms of power and money. Here we propose a technique to create diversity using an active material that can switch between an absorber and reflector and thus create alternative communications paths.

TABLE I. Median values of delay spread (ns) and path loss (dB) for different antenna orientations and presence or absence of bottom absorber.

Antenna Orientation	Absorber	
	None	Bottom
1	7.4 ns / 56.4 dB	5.3 ns / 58.1 dB
2	7.0 ns / 59.8 dB	6.5 ns / 61.3 dB
3	5.5 ns / 57.3 dB	1.7 ns / 58.3 dB

The layout of this paper is as follows. The characteristics of 60 GHz wireless communications in a cabinet are outlined in Section II. A ray-tracing and software simulation together with capacity performance results are presented in Section III. Further work is discussed in Section IV and a conclusion is drawn in Section V.

II. Channel Characteristics

A. Propagation environment within data center cabinet

The front section of the data-center cabinet has dimensions of 0.35 × 0.7 × 2.2 m as depicted in Fig. 1. The cabinet housing rack and rear are composed of steel, while the concrete floor of thickness 10.0 cm forms part of the bottom. The cabinet top-panel is assumed composed of absorber material of thickness 1 cm. The Tx and Rx dipole antennas are positioned at a distance of 4.0 cm from the server front. The four antennas of the Tx access point (AP) are centrally located, whilst four Rx dipoles are mounted on each of the 40 servers in the cabinet.

B. Effect of absorber and antenna orientation

The placement of radio wave absorber, together with the orientation of the dipole antenna affects the delay spread and propagation characteristics. By suitable arrangement of the electromagnetic wave absorbing material, the delay spread can be reduced, as also reported in [9] [10]. The position of absorber and its effect on the delay spread and path loss for three different orientations of the transmit and receive antenna was first investigated. Figure 2 shows the (top) delay spread and (bottom) path-loss for the case (left) without absorber on the top panel and (right) with absorber on the top panel. The delay spread is significantly reduced for the antenna Orientation 3 due to the main radiation being in the direction of the radio wave absorber. The absorber on the top panel reduces the median delay spread for Orientation 3 from 5.5 ns to 1.7 ns as shown in TABLE I. There is only a small increase in the corresponding pathloss from 57.3 dB to 58.3 dB with similar minor increases for the other antenna orientations. Due to the reduction in delay spread, the Orientation 3 was selected and used from hereon in the paper. The delay spread is considerably less than a cyclic period of, for example, OFDM mode of IEEE 802.11ad (48.4 ns) [11] and therefore the channel can be equalized without inter-symbol interference.

C. Introduction of active material

Along each side of the cabinet are three active-regions, which can switch between reflectors and absorbers, each of dimensions 66×35 cm as shown in Fig. 3. In a practical

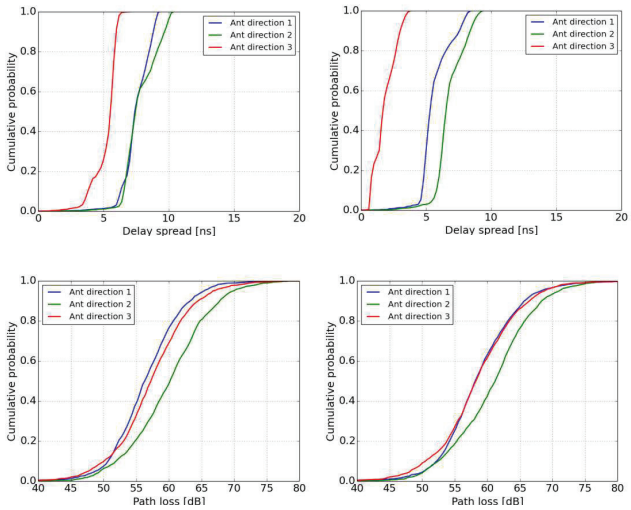

Fig. 2. (Top) Delay spread and (Bottom) Path loss for (left) Without absorber and (right) With absorber on top.

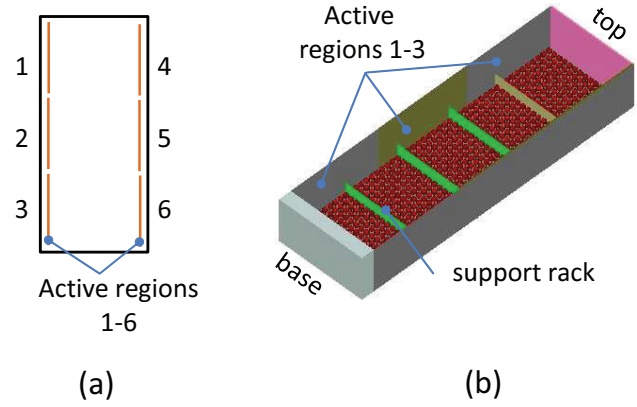

Fig. 3. (a) Cabinet front-view showing side-wall active regions 1-6, and (b) Wireless InSite™ Project View showing left-side active regions 1-3.

realization, the active-regions would be implemented as a meta-material such as described in [12] [13] which provide variability to the propagation channel [14]. Some of the active regions are inactive (absorbers) and the remaining are active (reflectors). By using such a material, the reflectivity and hence multipath characteristics can be adaptively controlled. In this work, when the active region is a reflector, the properties are modeled as those of 1 mm thick steel and when the region is inactive, the properties are modeled as an absorber with -23 dB reflection coefficient. The front door panel is composed of a steel mesh [15] with holes whose dimensions allow heat to escape the cabinet but EM radiation is reflected back for security reasons. A small absorber is placed on the front door covering 15% of the surface area in order to reduce the delay spread. Its size will be reduced as part of our future work.

The effect of the active regions can be seen from a plot of the signal direction of arrival (DoA), estimated using the Wireless InSite™ ray-tracing software [16]. The DoA at the arbitrarily chosen Rx position A (4.4 cm in x-dimension,

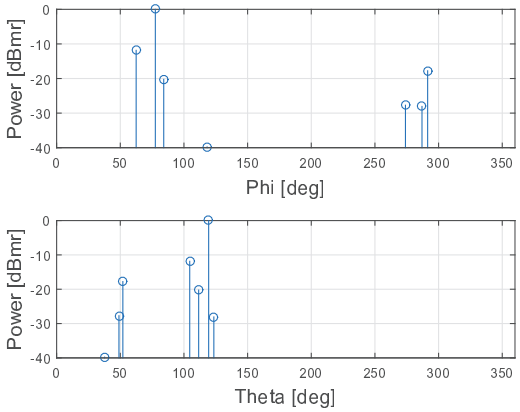

Fig. 4. Direction of arrival at Rx position A with active regions {2,6} active.
(Top) Phi, (Bottom) Theta orientations.

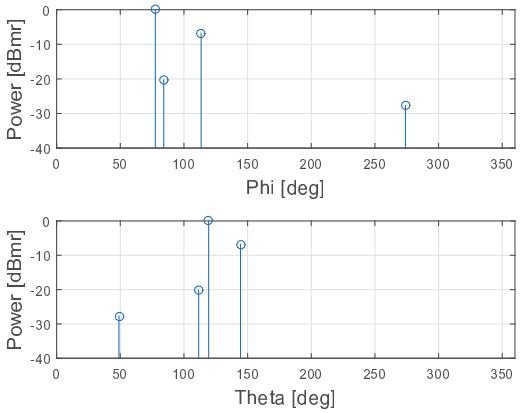

Fig. 5. Direction of arrival at Rx position A with active regions {3,4} active.
(Top) Phi, (Bottom) Theta orientations.

22.0 cm in y-dimension from the bottom left) is plotted for two regions active in positions {2,6} and {3,4} as shown in Figs. 4 and 5 respectively, where Theta is the angle relative to the z-axis (parallel to cabinet depth dimension) and Phi is the angle relative to the x-axis (parallel to cabinet width dimension). In both graphs a dominant LOS path is present but the reflected multipaths come from different directions. This results in decorrelation between the incident signals and can be exploited by a suitable receiver. The corresponding Wireless InSite™ Path View is plotted in Fig. 6 and shows the LOS and strongest reflected path from the center TX1 to Rx position A for the case of a bottom-right (a) reflector and, (b) absorber.

III. Capacity Simulation

In this section we describe the simulation set-up and post-processing of ray-traced data in order to estimate the capacity of each server.

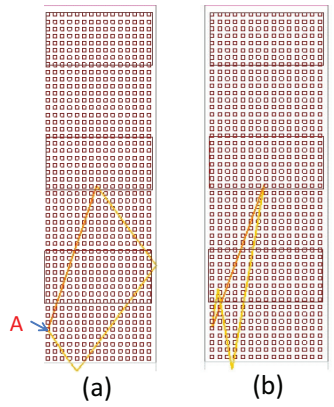

Fig. 6. Wireless InSite™ propagation path view showing LOS and strongest reflected path from center TX1 to Rx position A with bottom-right active region having (a) reflector and (b) absorber.

TABLE II. Simulation parameters.

Tx Antennas	4
Rx Antennas	4 per server
Servers (Rx arrays)	40
Rx array positions	12 (shifted on same row)
Sub-carriers	336
Active regions (Total 6)	0,1,2,6 are active (reflector) Remaining are inactive (absorber)
Combinations of active regions	23
SNR	20 dB

A. 60 GHz based solution

A 60 GHz solution has been identified as a candidate transmission technology for this work. As a starting point we have assumed that the PHY layer has the same channel bandwidth and transmit power as that used by the IEEE 802.11ad standard [11]. In this standard there are four 2.16 GHz channels that can employ the OFDM mode with 336 data sub-carriers. It is assumed each channel can connect 10 servers in a TDD scheme supporting the total 40 servers. By using 64QAM modulation in OFDM mode with low-density code rate (LDPC) rate=13/16, a 6.75 Gbps link can be achieved. Although, the 11ad scheme does not include a multiple-input multiple-output (MIMO) option, in order to increase the capacity we assume in our scheme that there are multiple antennas. By employing a 4×4 spatial multiplexing scheme, a theoretical maximum of 27 Gbps/rack or 2.7 Gbps/server (TDD mode) is possible, although this value will be lower in practice due to the existence of correlated channels, handshaking, and guard intervals, for example. Assuming the transmit power is set at 4 dBm, the noise figure is 6.5 dB with RF bandwidth of 2.16 GHz, pathloss is 58.3 dB (from TABLE I, antenna Orientation 3, absorber on the top panel), the received SNR is estimated at approximately 20 dB. The simulation parameters are summarized in TABLE II.

B. Ray tracing model

A plan-view of the cabinet showing the Tx and Rx element locations is in Fig. 7. The radio channel was measured at

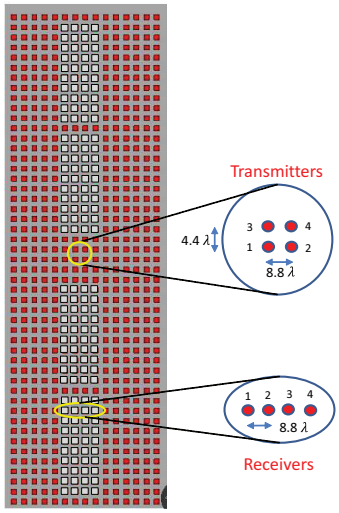

Fig. 7. Plan-view of Tx and Rx antenna positions within the cabinet. Rx array is shifted on same row. Rx1(Rx2) can occupy column positions 1-12(2-13) etc.

regular intervals of 4.4 cm (8.8λ) with 49 vertical and 15 horizontal Rx positions giving a total of 735 Rx measurement locations. The Tx elements are separated by 4.4 λ vertically and 8.8 λ horizontally (Note the Tx vertical grid spacing is half the Rx grid spacing). The servers are numbered 1 through 40 starting from the bottom. The servers are stacked on consecutive rows and thus at intervals of 4.4 cm and an extra row spacing is inserted between each of the four racks that support 10 servers. A linear-array of four Rx antennas is allocated to each server with an element spacing of 8.8λ. Through experiments it was found that a reasonably fair and even capacity distribution to each server was achieved when the transmit and receive antenna were in Orientation 3 i.e the dipole axis is parallel to the z-axis with reference to Fig. 1. The linear-array was shifted 1-12 positions along the same row increasing the experiment measurement data size.

A total of 23 different combinations of 'active region sets' were considered (TABLE II). Sets 1-15 comprise the 15 permutations of two regions being active out of the six positions. Set 16 is where all active-regions are active. Set 17 is where none of the active-regions are active. Sets 18-23 are where a single region is active.

The channel impulse responses were computed by the Wireless InSite^{TM} software from the Tx to each of the Rx elements by transmitting a sinusoidal signal. During post-processing, the responses were binned at the same sample rate as 802.11ad, i.e. 0.38 ns and the time-domain data was converted to frequency-domain using the 512-point FFT operator.

C. Eigenmode Transmission

The 4×4 channel on each sub-carrier is decomposed into two unitary matrices, **V** and **U** using singular value decomposition (SVD) as

$$\mathbf{H} = \mathbf{U}\ \mathrm{diag}\left[\sqrt{\lambda_1}, \sqrt{\lambda_2}, \sqrt{\lambda_3}, \sqrt{\lambda_4}\right] \mathbf{V}^{\mathrm{H}}, \qquad (1)$$

where λ_n is the n-th eigenvalue and $^{\mathrm{H}}$ is the Hermitian operator. The first eigenvalue is strongly dependent on the total received power and the LOS signal. Its value is almost the same regardless of the presence or absence of the active-reflector. A reflected signal has lower power and has only a small contribution to the first eigenvalue. The relative value of the 2nd eigenvalue will generally increase as the number of individual reflections increases.

D. Capacity

The capacity of each link depends on the spatial correlation of the signals impinging on the Rx array elements. There will therefore be a range of capacities depending on position, with some servers having a relatively high value whilst others having lower ones. At high SNR, the capacity is given by Eq. (2) [17] as

$$C = \Sigma_{k=1}^{r_H} \log_2 \left(1 + \frac{\mathrm{P}}{\sigma_n^2} \frac{\lambda_k^2}{r_H}\right), \qquad (2)$$

where r_H is the channel rank or number of non-zero singular values, σ_n^2 is the noise variance and P is a vector of substream transmit powers.

The optimized distribution of power on each eigenmode is determined by the water-filling algorithm depending on the substream SNR [17]. The received SNR is set at 20 dB based on the link-budget estimation in Section III A. The capacity is summed over the up to 4 active substreams on each sub-carrier. The capacity for each of the 40 servers is recorded at each sub-carrier and the process repeated with the Rx array shifted from 1-12 positions. The simulation is repeated for each of the 23 active-region sets. The capacities are plotted in Fig. 8 for the case of the array in the row-center depicted in Fig. 7. It can be seen that there is considerable variability across the active-region sets for the servers 1-15 and also servers 30-40 which are towards the bottom and top of the cabinet respectively. The capacities are more correlated across the central servers 15-25 and is considered due to a relatively stronger LOS Rician component dominating those of the multipath contributions. The particular capacity value depends on the exact spatial-position and the constructive-destructive signal additions, and therefore the service to a particular server could be optimized by careful selection of the active-region set. For example, the capacity for Server 14 can be increased from 11.8 bits/transmission with active-region Set 20 to 19.0 bits/transmission with active-region Set 16 as shown in Fig. 9.

The capacity cumulative distribution function (CDF) for each of the active-region sets is plotted in Fig. 10. At the median value (50% CDF level) it was found that the best set (Set 9) resulted in a capacity of 2.8 bits/transmission higher than that at Set 12 at 20 dB SNR. Set 9 is therefore considered the optimum set for the particular exact positioning of the Tx and Rx in the simulation. However, at 60 GHz an antenna displacement of just 0.125 mm results in a phase difference of 9.0 degrees. Such precise positioning is therefore not practical as a once-off in the manufacture/set-up stage and an adaptive scheme is proposed in order to find the best set. Furthermore, slight movement of the active-regions, introduction of foreign objects, metal heat expansion, etc will all contribute to a change in the optimum set. The active

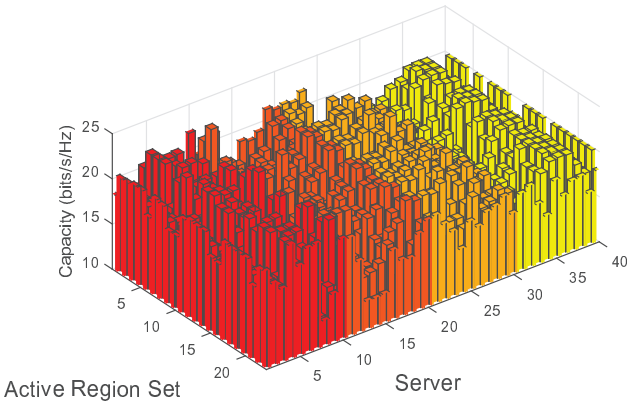

Fig. 8. Variation in capacity for each server for 23 active-region sets at 20 dB SNR. (Rx array is centered in each row as in Fig. 7).

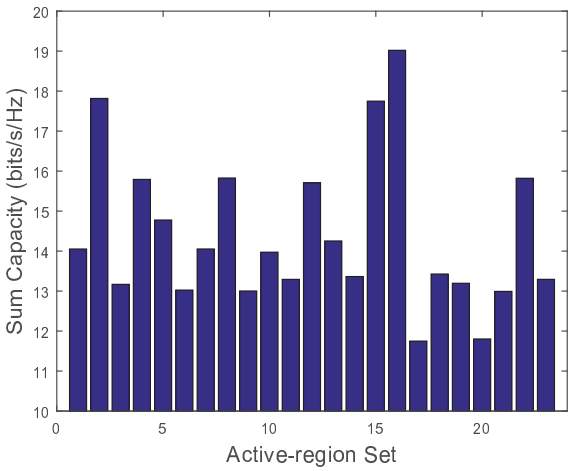

Fig. 9. Variation in capacity with active-region sets for Server 14 at 20 dB SNR (Centered Rx array)

regions could also be adaptively set and optimized for the traffic needs of each server. Although, it is not possible to model every small feature of the data-center cabinet, the adaptive scheme should reduce the need for exact antenna positioning and cabinet modeling in order to achieve good performance.

E. Condition number

In the ideal situation, the substream eigenvalues would have the same value. The condition number (CN) is the ratio of the maximum to minimum eigenvalue and is a useful indicator of the how well the channel matrix is conditioned. It is expressed at each sub-carrier, i as Eq. (3)

$$CN^i = \frac{\lambda^i_{max}}{\lambda^i_{min}} \tag{3}$$

A matrix is considered well-conditioned when the CN is less than about 10 dB, whereas above this value detection becomes

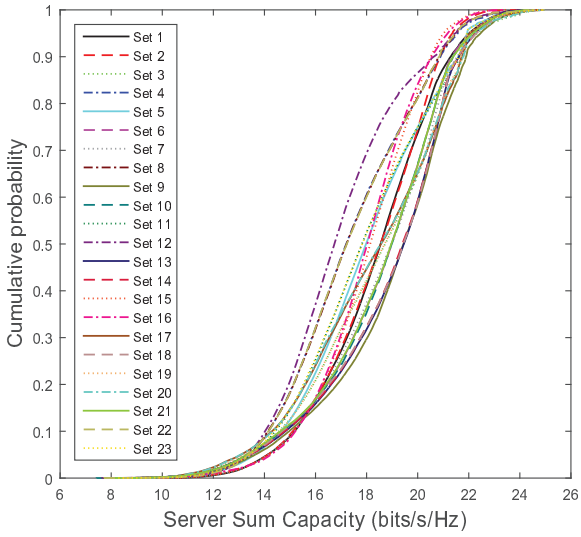

Fig. 10. CDF of capacity to all servers for each of the active-region sets at 20 dB SNR

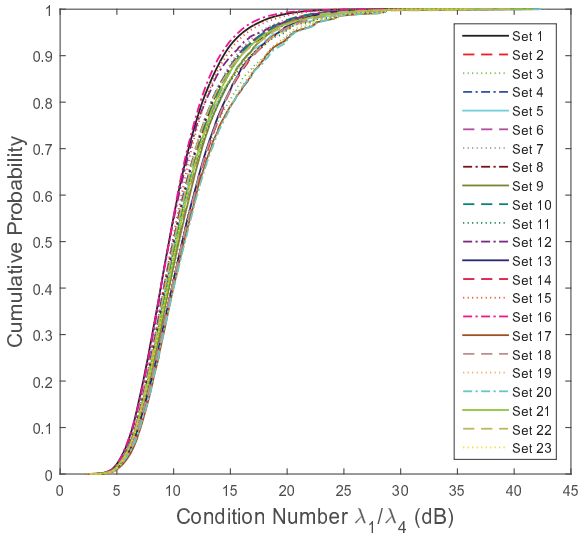

Fig. 11. CDF of condition number for each active-region set compiled over all sub-carriers and servers.

more sensitive to errors in the channel estimation [18]. CDF results show that 58% of the channels for active-region Set 1 has a condition number less than 10 dB as shown in Fig. 11. As the condition number increases, the required SNR to maintain a given level of performance also increases. The calculation of the CN requires little complexity overhead in a practical system in which the channel state information is already computed and the CN value could be used to control the active-region switching. For example, if the CN is less than a 10 dB threshold, the active region set is considered good, and otherwise an alternative configuration can be tried.

IV. Further Work

As part of further work, we plan to investigate an adaptive scheme in which the configuration of the active regions is dependent on the condition number. The orientation of the receive antennas relative to their position in the cabinet will be studied. The relative number and size of the active-regions should be considered as it will impact on the cost of materials. The ray-traced channel model should be verified through measuring the actual S parameters with a vector network analyzer. Finally, an appropriate number of active-region sets necessary for the calibration routine should be estimated in order to minimize the complexity.

V. Conclusion

A 60 GHz wireless communication system has been proposed as a replacement for Ethernet cables in the data-center cabinet. Due to the static channel, a method to create channel diversity using active-regions was investigated. Performance results derived from a ray-tracing simulation showed that the capacity could be increased by 2.8 bits/s/Hz at an SNR of 20 dB at the median value. The technique of applying adaptive regions to create diversity can be applied to almost any wireless communications system. It is particularly beneficial when there is little or no movement within the channel environment such as in a cabinet, box or empty room. The adaptive scheme should also reduce the requirement of precise antenna positioning in order to achieve good performance.

Acknowledgment

This work is supported in part by Japan Ministry of Internal Affairs and Communications with the SCOPE fund No. 145001101 for ”Research and development into data-center rack cable reduction using wireless communication leading to air conditioning efficiency improvement.”

References

[1] W. Heddeghem, S. Lambert, B. Lannoo, D. Colle, M. Pickavet, and P. Demeester, “Trends in worldwide ICT electricity consumption from 2007 to 2012,” *Computer Communications* , 2012.

[2] M. Bari, R. Boutaba, R. Esteves, L. Granville, M. Podlesny, et al., “Data Center Network Virtualization: A Survey,” *IEEE Commun. Surv. & Tut.*, Vol. 15, No. 2, 2013.

[3] Cisco, “Cisco Nexus 9500 Platform Switches,” *Datasheet*, pp. 1–16, 2015.

[4] C. Marcu, D. Chowdhury, C. Thakkar, J. D. Park, L. Kong, et al. “A 90 nm CMOS Low-Power 60 GHz Transceiver With Integrated Baseband Circuitry,” *IEEE Journal of Solid State Electronics*, vol. 44, no. 12.

[5] K. Okada, K. Matsushita, K. Bunsen, R. Murakami, A. Musa, T. Sato et. al, “A 60GHz 16QAM/8PSK/QPSK/BPSK direct-conversion transceiver for IEEE 802.15.3c,” *IEEE International Solid-State Circuits Conference Digest of Technical Papers (ISSCC)*, pp. 160–162, 2011.

[6] Y. Katayama, K. Takano, Y. Kohda, N. Ohba, and D. Nakanoet, “Wireless Data Center Networking with Steered-Beam mmWave Links,” *IEEE WCNC* , 2011.

[7] Y. Katayama, T. Yamane, Y. Kohda, K. Takano, D. Nakano, and N. Ohba, “MIMO Link Design Strategy for Wireless Data Center Applications,” *IEEE WCNC* , 2012.

[8] M. Chen, H. Jin, Y. Wen, and V. Leung, “Enabling Technologies for Future Data Center Networking- A Primer,” *IEEE Network Magazine*, Jul. / Aug. 2013.

[9] S. Khademi, S. Chepuri, Z. Irahhauten, G. Janssen, and A. van der Veen, “60 GHz Wireless Link Within Metal Enclosures: Channel Measurements and System Analysis,” *Cornell University Library*, Nov. 2013

[10] A. Matsubara, T. Ichikawa, et al., “Measurements and Characterisation of Ultra Wideband Propagation within Spacecrafts,” *Loughborough Antennas and Propagat. Conf.*, Nov. 2009.

[11] L. Verma, M. Fakharzadeh, S. Choi, “WiFi on Steroids: 802.11AC and 802.11AD,” *IEEE Wireless Communications Magazine*, Dec. 2013

[12] F. Bilotti and L. Vegni, “Design of Metamaterial - based Resonant microwave Absorbers with Reduced Thickness in,” *Meta-materials and Plasmonics: Fundamentals, Modeling, Applications. Springer*, vol. 99, pp .165–174, 2009.

[13] B. Zhu, K. Chen, N. Jia, L. Sun, et al., “Dynamic Control of Electromagnetic Wave Propagation with the Equivalent Principle Inspired Tunable Metasurface,” *Nature - Scientific Reports*, pp .1–7, May 2014.

[14] J. Shen, Y. Oda, T. Furuno, T. Maruyama, and T. Ohya, “A Novel Approach for Capacity Improvement of 2×2 MIMO in LOS Channel Using Reflectarray,” *Proc. IEEE VTC 2011*, 2011.

[15] H. Kawaguchi, M. Ueba, and M. Matsuoka, “FDTD Analysis of Millimeter Wave Data Communication between Data-servers in Server-rack,” *Proc. of the 20th International Conference on the Computation of Electromagnetic Fields (COMPUMAG 2015) (Accepted for publication)*, Montreal, Canada, June 2015.

[16] Remcom, “Wireless InSite - Site-specific Radio Propagation Prediction Software,” *User’s Manual*, v. 2.5.14, Mar. 2010.

[17] C. Oestges, and B. Clerckx, “MIMO Wireless Communications,” *Elsevier*, 2007.

[18] Agilent, “MIMO Performance and Condition Number in LTE Test,” *Application Note*, Oct. 2009.